ORIGINAL RESEARCH

A Compact Non-Planar Coil Design for the SFLM Hybrid

A. Hagnestål · O. Ågren · V. E. Moiseenko

Abstract A non-planar single layer semiconductor coil set for a version of the Straight Field Line Mirror Hybrid concept with reduced magnetic field has been computed. The coil set consists of 30 coils that are somewhat similar to baseball coils with skewed sides. The coil set has been modeled with filamentary current distributions and basic scaling assumptions have been made regarding the coil widths. This coil set is expected to be considerably cheaper than a previous computed coil set. The coils can probably be produced with technologies known today.

Keywords Superconducting coils · Hybrid reactor · Fusion · Fission · Mirror machine · Transmutation

Introduction

A design of superconducting coils [1] for the Straight Field Line Mirror (SFLM) hybrid concept [2] has been made in an earlier work with semi-planar coils for a midplane vacuum magnetic field B_0 of 2 T and a mirror ratio of four. This paper presents a design of a non-planar superconducting coil system for the SFLM hybrid concept where B_0 has been reduced from 2 to 1.25 T and the maximum midplane β has been increased from about 0.2 to about 0.5. The main reason for the new design is to reduce the cost

and size of the coils. With the new coil design, a single layer of coils will be sufficient to produce the magnetic field while the old coil system had two layers. Since the magnetic field strength is now reduced, the sizes of the coils are significantly reduced and most coils can be made of NbTi instead of Nb_3Sn or Nb_3Al, which will reduce the cost of the coils substantially. Manufacturing of non-planar coils has been made for the Wendelstein $7\times$ stellarator [3], and is considered to be a known technology.

The fusion-fission reactor (hybrid reactor) is a combination of a fusion reactor and a fast fission reactor, where the fusion reactor is used as a neutron source for the surrounding subcritical fission core. The fusion neutrons trigger fission reactions in the fission core which produces fission neutrons, and on average a cascade of fission neutrons and subsequent fission reactions will be created for each fusion neutron. Thereby, the fission core will act as a strong energy multiplier for the fusion reactor, and a fission to fusion power ratio of about 100–150 is possible with a fusion mirror machine driver [4] in steady-state mode. A subcritical fission core is a fission core with an effective neutron multiplication factor K_{eff} of less than unity, typically 0.9–0.97. Such a core is not self-sufficient in neutrons, and must have an external neutron source to produce energy. Systems with subcritical cores and external neutron sources are called driven systems. The aims of hybrid reactors are energy production, breeding of fertile fissile material from U-238 or Th-232 or transmutation (by fission) of TRansUranic (TRU) elements in radioactive waste from fission plants. Competitors to hybrid reactors are ADS (Accelerator-Driven Systems) and fast fission reactors, but even LWRs (Light Water Reactors) can transmute TRU to some extent (plutonium).

The reason to study mirror machines for hybrids is the steady-state option and the simple geometry, which allows

A. Hagnestål (✉) · O. Ågren
Ångström Laboratory, Division of Electricity, Uppsala University, Box 534, 751 21 Uppsala, Sweden
e-mail: Anders.Hagnestal@Angstrom.uu.se

V. E. Moiseenko
Institute of Plasma Physics, National Science Center "Kharkov Institute of Physics and Technology", Akademichna st. 1, 61108 Kharkiv, Ukraine

access to the plasma from the mirror ends and reduces fusion neutron leakage through holes in the fission mantle. The concern for insufficient plasma confinement is a less serious concern for a mirror hybrid than for a pure fusion device.

The hybrid reactor is an old concept that dates back to the 1950:ies, and among others the following scientists have contributed to progress in the field. Bethe [5] and others advocated the concept in the 1970:ies, see also Ref. [6]. Moir et al. at Lawrence Livermore studied mirror-based (and other) hybrids in 1970–1980:ies [7], and made significant contributions to the field with various design studies. The easiest way to find documents related to this is via Moirs homepage [8]. Taczanowski [9] contributed with studies on tandem mirrors in the 1990:ies and Manheimer [10] and others discussed and analyzed the subject later on. In the new millennia there has been a renewal of the interest in fusion hybrids, and the idea is being persued by several groups. To the authors' knowledge, the following groups are studying fusion hybrids or related issues:

- Stacey et al. [11] at Georgia Tech who have studied several tokamak-based concepts with downscaled ITER parameters.
- Wu et al. [12] in China who studies tokamak-based hybrids (several FDS concepts) and are putting large resources into hybrid studies.
- Kotschenreuther, Mahajan et al. [13] of Institute for Fusion Studies who studies spherical tokamak-based hybrids.
- Gryaznewich et al. at Culham Laboratory is examining the possibilities to use spherical tokamaks as neutron sources.
- Researchers at Budker Institute who studies a mirror-based hybrid scenario using the axisymmetric Gas Dynamic Trap (GDT) as a driver [14].
- Moiseenko et al. in Kharkiv, Ukraine is working on fusion-fission and neutron sources [15].
- Moir et al. [16] at Lawrence Livermore who recently presented an axisymmetric mirror-based concept.

- Taczanowski et al. [9] has some activities in fusion-fission.
- Yapici et al. [17] are working with fusion-fission using catalyzed fusion as a driver.
- Manheimer [10] is advocating fusion-fission.
- An Uppsala University group (the authors) are evaluating quadrupolar single cell mirror fusion-fission hybrids [2].

In section "Geometry", the geometry of the device is described. Section "The Vacuum Magnetic Field" describes the properties of the vacuum magnetic field. Section "Coil Parameterization" describes the coil type used. Section "Coil Optimization" describes the coil optimization procedure. The results and discussion is in section "Results and Discussion" and section "Conclusion" concludes the paper.

Geometry

In this section, the geometric constraints for the coil system are briefly described. The geometry of the vacuum chamber, fission mantle, shielding etc. in the confinement region is changed from the previous coil design described in Ref. [1] in two ways. Outside the confinement region, the vacuum chamber radius is expanded to 1 m close to the confinement region and expands more towards the ends. This is since the magnetic field strength drops off in this region before the flux tube has been recirculated, giving a somewhat larger flux tube outer radius. Also, the space allocated in Ref. [1] for neutron shielding was too thin on the old design. A redesign of the fission mantle has been made, and at this stage the fission mantle with shielding has an outer radius of 199.8 cm [18]. Thereby, the inner coil radius of 210 cm which was used in the old coil system can be used here as well which provides some extra space for expanding the neutron shield if this should prove necessary.

The geometric properties of the reactor are shown in Fig. 1. The vacuum chamber is cylindrical in the confinement region, and expands axisymmetrically at the magnetic

Fig. 1 The device without a coil system in 3D (**a**) and the cross section of the confinement region (**b**)
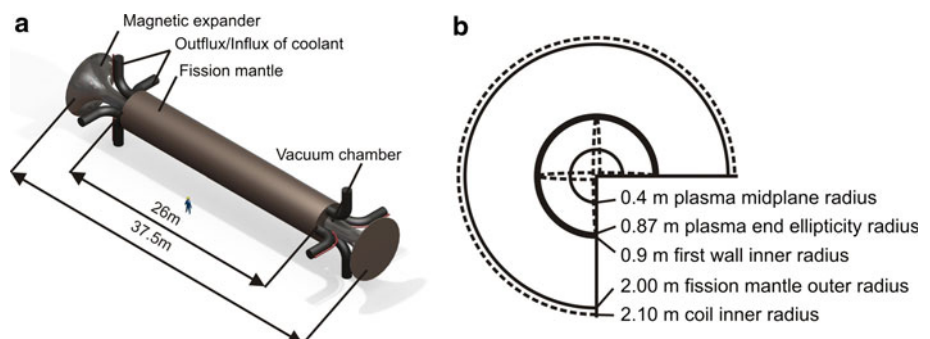
expanders located at the two longitudinal ends of the device. Between the magnetic expanders and the confinement region, two recirculation regions are located which have a somewhat larger vacuum chamber radius than the confinement region. The purpose of these regions is to recirculate the flux tube and give axisymmetric magnetic expanders. The 26 m long fission mantle surrounds the vacuum chamber at the confinement region, and a more detailed description can be found in Ref. [4] and Ref. [18]. The coolant influx/outflux that somehow must pass through the layer of coils is represented by the pipes from the fission mantle in Fig. 1, and sufficient spacing between the coils to fit them in must be allocated in the coil optimization somewhere in the recirculation regions.

A simple model for the coil sizes are used, where the cross sectional area of the winding packs (including the jacket) are assumed to be proportional to the current. The current density of 2,280 kA/(29.5 × 29.5 cm^2) = 2.6 kA/cm^2 is approximately taken from the design of the toroidal field superconducting coils of JT-60SA, which uses NbTi coils and have a magnetic field modulus similar to that of this device [19]. The coil structure material that surrounds the winding pack will also occupy some space. This is roughly accounted for by adding 10% of the coil width at each side, expanding the coil sides with a factor 1.2. This is roughly in accordance with Ref. [19]. For simplicity, the coil cross sections are made quadratic.

The Vacuum Magnetic Field

The prescribed shape of the vacuum magnetic field in the confinement region has not been significantly modified from the previous coil design, and is described in more detail in Ref. [1]. The shape of the recirculation region has, however, been modified. The modulus of the magnetic field has been lowered to 5/8 of the previous field in the whole device to 1.25 T at the midplane to reduce the cost of the coil system. The vacuum magnetic field is expressed in the long-thin (paraxial) approximation with $\lambda = a/c$ as small parameter, where a is the plasma radius and $2c$ is the length of the confinement region. To order $o(\lambda^3)$ the magnetic field is described by two functions, the axisymmetric field $\tilde{B}(z)$ which is the magnetic field at the z axis and the quadrupolar field which is represented by the function $g(z)$. The magnetic field components are then

$$B_x = \frac{x}{2}(g - \tilde{B}'), \tag{1}$$

$$B_y = -\frac{y}{2}(g + \tilde{B}') \tag{2}$$

$$B_z = \tilde{B} + \frac{x^2}{4}\frac{d(g - \tilde{B}')}{dz} - \frac{y^2}{4}\frac{d(g + \tilde{B}')}{dz} \tag{3}$$

where prime denotes differentiation with respect to z. To ensure flute stability in the low β limit the flute stability criterion from Ref. [20], Eq. (49),

$$\int_{-z_{end}}^{z_{end}} \hat{p}\frac{\kappa_\psi}{B}dz \geq 0 \tag{4}$$

$$\hat{p} = (\hat{p}_\perp + \hat{p}_\parallel)/2 \tag{5}$$

is used. This corresponds to [1, 20]

$$W_{1,2}(z_{end}) = \int_{-z_{end}}^{z_{end}} \frac{\hat{p}dz}{\tilde{B}(z)}e^{2\int_0^z h_{1,2}(z')dz'}\left[h_{1,2}^2(z) + \frac{dh_{1,2}(z)}{dz}\right] \geq 0 \tag{6}$$

in the near axis approximation, where

$$h_1(z) = \frac{g - \tilde{B}'}{2\tilde{B}} = \frac{1}{\tilde{B}}\frac{B_x}{x} + O(\lambda^2) \tag{7}$$

$$h_2(z) = -\frac{g + \tilde{B}'}{2\tilde{B}} = \frac{1}{\tilde{B}}\frac{B_y}{y} + O(\lambda^2) \tag{8}$$

Due to symmetry, $W_1 = W_2$ and thus $W_1 \geq 0$ is sufficient for stability. The pressure function $\hat{p}$ is independent of radius and is here chosen as a simple normalized representative sloshing ion distribution just like in Ref. [1]. The flux tube ellipticity is

$$\varepsilon_{ell} = \max\left(\frac{x_{max}(z)}{y_{max}(z)}, \frac{y_{max}(z)}{x_{max}(z)}\right)$$
$$= \max\left(e^{\int_0^z \frac{g(z')}{B(z')}dz'}, e^{-\int_0^z \frac{g(z')}{B(z')}dz'}\right) \tag{9}$$

By tracing field lines from a circular midplane outer plasma boundary with radius a, the radially outermost field line determines a minimal value for the vacuum tube inner radius $r_{vc,min}(z)$,

$$r_{vc,min}(z) = a\sqrt{\frac{\varepsilon_{ell}(z)B_0}{\tilde{B}(z)}} \tag{10}$$

It is necessary to check from this formula that that the plasma surface does not intersect the vacuum chamber first wall.

The prescribed vacuum field used as a reference in this work is presented in Fig. 2, and is the same as in Ref. [1] save for a factor of 5/8 in B. The field is specified by the functions $\tilde{B}(z)$ and $g(z)$, and the flute stability integral W_1, the associated pressure function and the flux tube ellipticity is shown.

Coil Parameterization

The 3-dimensional coil type chosen, which we here name fish-bone coil due to the similarity of a fish skeleton when
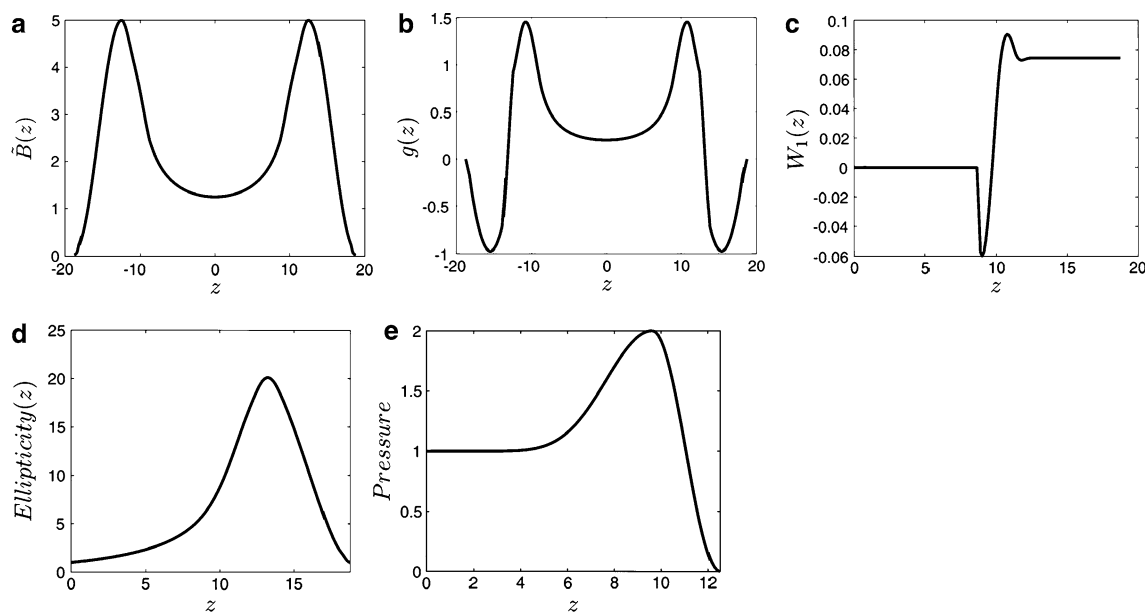
Fig. 2 The vacuum field properties, with the axisymmetric field $\tilde{B}(z)$ in (**a**), the $g(z)$ function in (**b**), the pressure weighted W_I stability integral in (**c**), the flux tube ellipticity in (**d**) and the pressure function used in the W_I integral in (**e**)
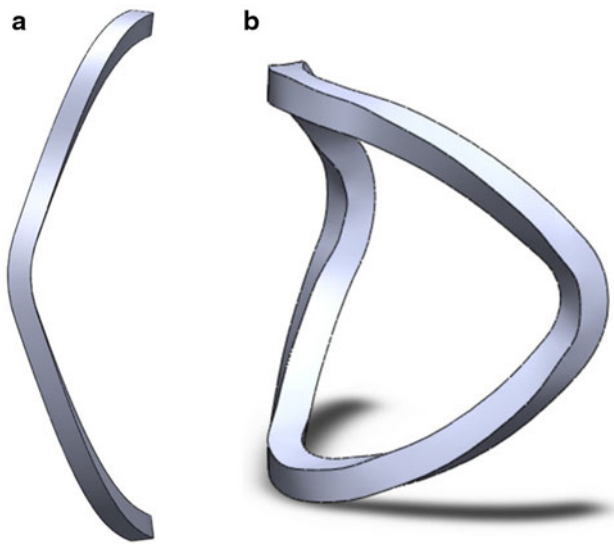

Fig. 3 The fish-bone 3-dimensional coil type used in the coil set from two different angles

several coils are added, is shown in Fig. 3 in 3D. The coil type produce both an axisymmetric magnetic field and a quadrupolar field.

In mirror machines, the quadrupolar field is often created by a combination of Ioffe bars, baseball coils [21] and yin-yang coils [22], possibly combined with racetrack coils (roughly elliptical planar coils) or similar. The coils chosen here somewhat resembles baseball coils with skewed sides. Yin-Yang coils are less effective at producing a quadrupolar field when there is a thick fission mantle or an almost

equally thick fusion neutron shield inside the coil. The coil geometry is best described by looking at the circumferential surface that the coil is oriented on. The parameterized curve that describes a current thread in the coil is at a constant distance from the z axis. Thus, the curve is well described using cylindrical coordinates (r, φ, z) with r kept constant for each filament. The coil layout on that circumferential surface is shown in Fig. 4.

Half the coil is shown, and the curve consists of straight lines and circle segments in that plane. Such a curve can be parameterized using H, L and a from Fig. 4, where a is the radius of the circle segments and a negative L wraps the coil so that a positive coil contribution to $\tilde{B}$ gives a negative coil contribution to g. From the symmetry, we get $H = r\pi/2$ since H is one quarter of the circumference. To parameterize the curve, it is convenient to express the distances c and d in Fig. 4 in L, H and a and the angle α in d and a. Within reasonable values of H and a ($H > 2a$),

$$d = \frac{aH^2 + aL^2 - \sqrt{a^2H^2(H^2 + L^2 - 4a|L|)} - 2a^2|L|}{4a^2 + H^2 + L^2 - 4a|L|},$$
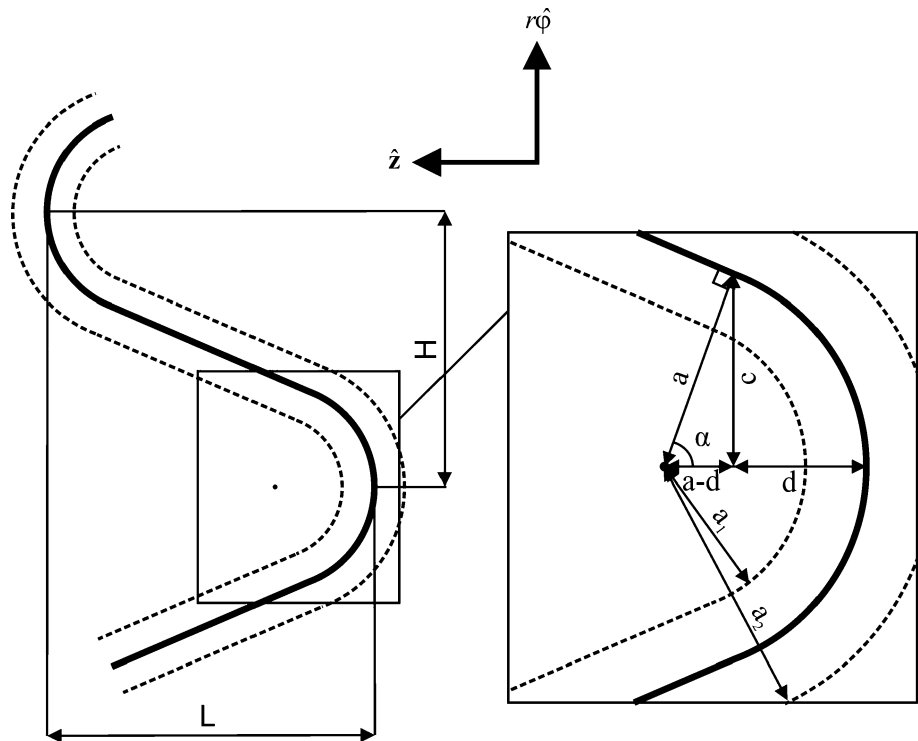(11)

$$c = \sqrt{a^2 - (a - d)^2}$$
(12)

and

$$\alpha = \cos^{-1}\left(\frac{a - d}{a}\right)$$
(13)

Each coil is divided into ($m \times m$) current filaments. To parameterize the filament curve it is divided into 8

Fig. 4 The coil layout on the circumferential surface that wraps the fission mantle

subsections, 4 straight lines and 4 circle segments (on the flattened out circumferential surface). For two filaments that have different z positions the radii of the circle segments differ (see Fig. 4). Also, for all filaments except those that are in the coil midline in z, the radii of the circle segments varies along the curve where 2 circle segments have radii a_1 and 2 circle segments have radii a_2 (see Fig. 4). In the parameterization, $n \in \{0,1,2,3\}$ where each number represents one quadrant of the coil and to simplify we define

$$\sigma_n = \begin{cases} 1 & \text{for even } n \\ -1 & \text{for odd } n \end{cases} \tag{14}$$

$$\sigma_L = \frac{L}{|L|} \tag{15}$$

The filament circle segments are parameterized with the curve parameter t as

$$a_{eff} = a - \sigma_n \Delta z, \tag{16}$$

$$\varphi(t) = n\frac{\pi}{2} + \frac{a_{eff}}{r} \sin\left(\frac{t - t_{max}/2}{t_{max}/2}\alpha\right) \tag{17}$$

$$x(t) = r\cos[\varphi(t)], \tag{18}$$

$$y(t) = r\sin[\varphi(t)], \tag{19}$$

$$t \in [0, t_{max}] \tag{20}$$

$$z(t) = \sigma_n\left(\sigma_L a_{eff}\left[1 - \cos\left(\frac{t - t_{max}/2}{t_{max}/2}\alpha\right)\right] - \frac{L}{2}\right) + \sigma_L \Delta z_l + z_0 \tag{21}$$

and the filament line segments are parameterized as

$$\Delta\varphi = \Delta z \sin\alpha, \tag{22}$$

$$\Delta z_l = \Delta z \cos\alpha \tag{23}$$

$$\varphi(t) = n\frac{\pi}{2} + \frac{1}{r}\left[c + \frac{t}{t_{max}}(H - 2c) - \sigma_n\Delta\varphi\right] \tag{24}$$

$$x(t) = r\cos[\varphi(t)], \tag{25}$$

$$y(t) = r\sin[\varphi(t)], \tag{26}$$

$$t \in [0, t_{max}] \tag{27}$$

$$z(t) = \sigma_n\left[\sigma_L d - \frac{L}{2} + \frac{t}{t_{max}}(L - \sigma_L 2d)\right] + \sigma_L \Delta z_l + z_0 \tag{28}$$

where $\Delta z < a$ represents the filament displacement in z from the coil central filament, z_0 is the coil center z position and r is the radial distance to the filament from the z axis.

Coil Optimization

To find a coil set based on the coil type described in section "Coil Parameterization" which reproduces the predefined magnetic field, an array of parameterized such coils were set up. In total, 30 coils were used, 15 on each side of the midplane. The coil system has a symmetry in the midplane, where each coil at position z has a corresponding oppositely located coil at $-z$. This corresponding coil is, however, not mirrored in shape, and both coils have the

same geometric shape and the same current. To find a magnetic field in the long-thin approximation, the 15 coil pairs should reproduce the prescribed functions $\tilde{B}(z)$ and $g(z)$. The coil pairs are parameterized using z, L, r_i, a, and I, where r_i is the inner radius of the coil, $\pm z$ is the coil center positions and I is the current. The current I controls the overall magnetic field contribution from the coil and thereby more or less controls $\tilde{B}(z)$. The parameter L controls (in combination with I) the contribution to the $g(z)$ function (where a negative L gives a wrapped coil and a negative contribution to $g(z)$), although it also slightly affects the distribution of $\tilde{B}(z)$. The contribution to the functions $\tilde{B}(z)$ and $g(z)$ for one coil are shown in Fig. 5. Note that the contribution to $g(z)$ is more localized in z than the contribution to $\tilde{B}(z)$, which in this respect makes it a bit harder to find an accurate reproduction of a varying $\tilde{B}(z)$ than of a varying $g(z)$ with a coil set. On the other hand, space requirements limit the variation in L between adjacent coils.

By the obvious demand that r_i should be kept as small as possible to save current, r_i is set to 2.10 m for all coils except the circular cusp coils at the magnetic expanders which have $r_i = 3$ m due to the large plasma radius at the magnetic expander. Also, the parameter a is preset for all coils (to 1 m for all coils). Thereby, the varying parameters for each coil pair are z, L and I. There is also a constraint that the coils should not intersect. The coils are formed so that they can be inserted into each other like a pile of drinking glasses. In practice, this limits the variation of the L parameter along the coil set and sets restrictions on the optimization process. The problem now looks like a straightforward optimization problem to solve with a local optimizer to find the parameters for the coils in a similar manner as has been done in [1]. It proved, however, to be sufficient to optimize the coils by hand, which was quite easily done since the parameters are so well separated in the sense that one parameter more or less controls each function $\tilde{B}(z)$ and $g(z)$. The hand optimization gave more practical solutions than the attempted numerical optimizations that were investigated.
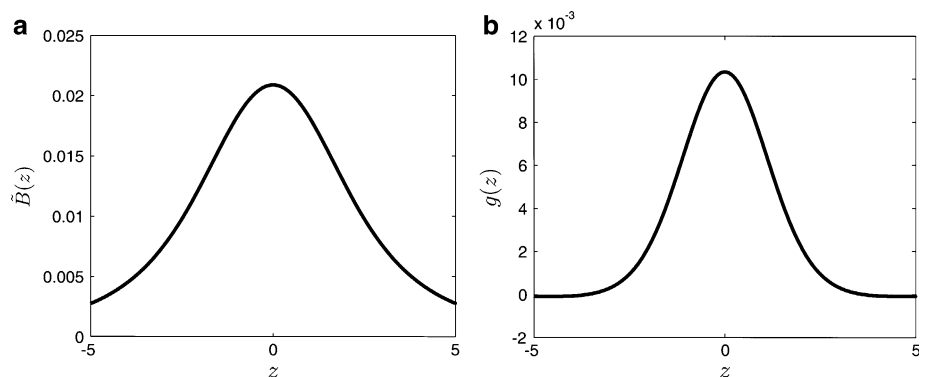
Results and Discussion

A number of properties of the magnetic field that would be produced by the coil set are shown in Fig. 6. The deviation from the ideal field (see Fig. 2) in the confinement region is shown in Fig. 6a for $\tilde{B}(z)$ and Fig. 6b for $g(z)$. The maximum deviation in $\tilde{B}(z)$ is about 2.5%, which partly arises from a smoothening of a somewhat poor concatenation point between the SFLM field and the ending field at $|z| = 8.75$m [1]. For $g(z)$, the typical deviation is below 1% except near the mirror end where the quadrupolar field deliberately has been made weaker to lower the flux tube ellipticity. This does not have a significant effect on the flute stability function W_I, since the plasma pressure is low in this region. Figure 6c shows the $\tilde{B}(z)$ function and Fig. 6d shows $g(z)$. In the recirculation region and the magnetic expander, the ideal field profile from Ref. [1] and Fig. 2 is only very roughly followed. The field that would be produced by the coils has, however, similar properties in this region. In Fig. 6e, the pressure weighted stability function W_I in the confinement region is shown and compared with that of the ideal field. There is a stability margin to flutes in the low β limit, since $W_1(z = 12.5) > 0$. In Fig. 6f, the flux tube ellipticity is shown. The maximum ellipticity is about 19.4, which is somewhat lower than in Ref. [1] since $g(z)$ has been slightly modified. The recirculation region reduces the ellipticity to about 1 at the magnetic expanders and makes the plasma receiving "divertor plates" circular. With a midplane plasma edge radius of $a = 40$ cm, the outermost plasma edge $r_{vc,min}(z)$ is calculated for the coil set using (10). The result is shown in Fig. 6g, and a magnification of the mirror end region for $r_{vc,min}(z)$ is shown in Fig. 6h. At the mirror end ($z = 12.5$), the outermost plasma edge radius is 87 cm. At about $z = 13.5$ in the recirculation region a maximum of about 93 cm is reached, which illustrates the need to expand the vacuum chamber beyond the mirror ends. At the end of the magnetic expander, $r_{vc,min}(18.75) \approx 4$ m.

The resulting coil set is described in Table 1. The C-14 coils are the recirculation coils and have a negative L

Fig. 5 The contribution to the functions $\tilde{B}(z)$ (**a**) and $g(z)$ (**b**) for one coil with parameters $a = 1$ m, $r = 2.3$ m, $z = 0$ m, $L = 2$ m and $I = 100$ kA. The field is calculated with a single filament at the center of the coil

Fig. 6 The components and some properties of the magnetic field that would be generated by the coil set. The figures show the deviation from the ideal field of $\tilde{B}(z)$ in the confinement region in (**a**) and $g(z)$ in (**b**), $\tilde{B}(z)$ in (**c**), $g(z)$ in (**d**), the $w_1(z)$ stability function in the confinement region in (**e**), the flux tube ellipticity in (**f**) and the outermost plasma edge radius $r_{vc,min}(z)$ in (**g**) and (**h**)
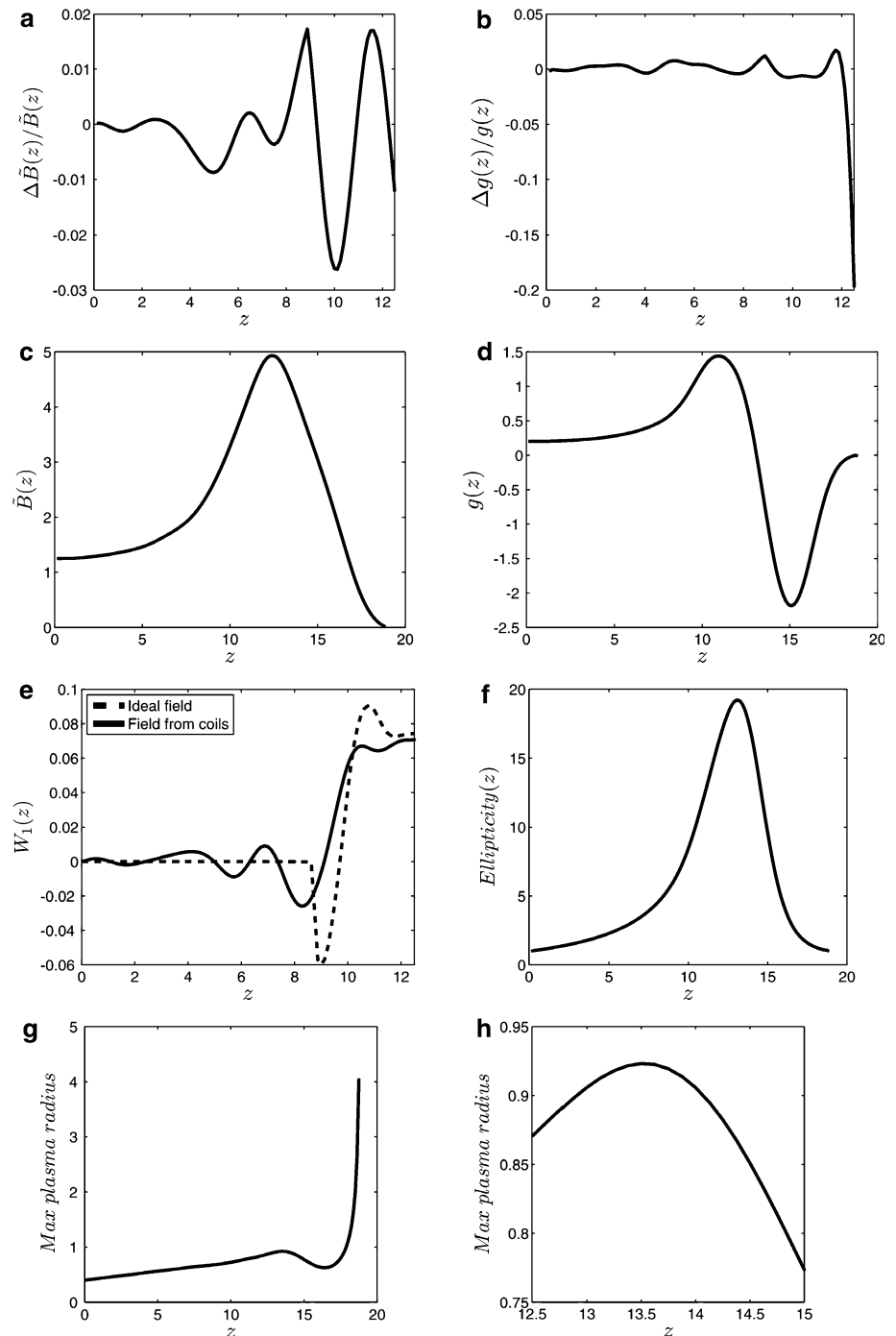
which gives a wrapped coil that produces a negative contribution to $g(z)$ for a positive contribution in $\tilde{B}(z)$. The C-15 coils are the cusp coils which have a negative current that gives a negative contribution to $\tilde{B}(z)$. The C-15 coils are circular ($L = 0$). The coils do not intersect other coils or other parts of the device, at least not significantly (only possibly very slightly in the structure material, which can be handled in a detailed design).

The resulting coil system is also shown in 3D in Fig. 7, where only the coils are shown in (a) and the vacuum chamber, fission mantle and the coolant influx/outflux has been added in (b).

To replace the old coil set with the new one with the weaker field has several advantages. One can easily be seen in Fig. 8, where the outer radii of the largest coils of the two coil systems are shown. As seen, the new outer coil radius

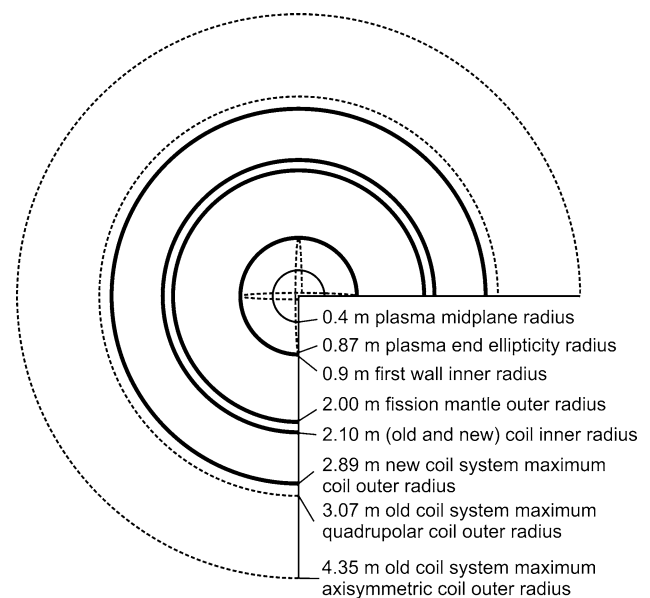**Table 1** The 3D coil parameters on the $z > 0$ side of the midplane

Coil name	z(m)	I(kA)	L(m)	r(m)	a(m)	Coil width (m)
C-01	0.4	787	0.915	2.1	1	0.209
C-02	1.25	700	1.085	2.1	1	0.197
C-03	2	700	0.905	2.1	1	0.197
C-04	2.75	710	1.05	2.1	1	0.198
C-05	3.5	762	1.035	2.1	1	0.205
C-06	4.25	720	1.06	2.1	1	0.200
C-07	5	680	1.20	2.1	1	0.194
C-08	5.75	750	1.68	2.1	1	0.204
C-09	6.5	1,100	0.88	2.1	1	0.247
C-10	7.7	1,640	2	2.1	1	0.301
C-11	9.5	2,750	2.33	2.1	1	0.390
C-12	11	5,600	2.32	2.1	1	0.557
C-13	12.45	11,150	0.71	2.1	1	0.786
C-14 (recirculation)	15.05	11,200	−2.98	2.1	1	0.788
C-15 (cusp)	17.4	−5,070	0	3	1	0.530
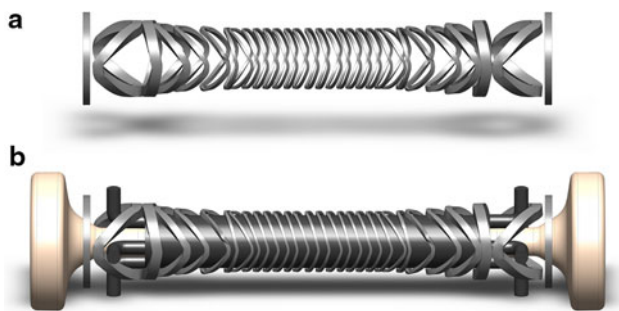
Fig. 7 The resulting coil system in 3D, where the coils are shown in (**a**) and the coils with the vacuum chamber, fission mantle and coolant influx/outflux are shown in (**b**)

0.4 m plasma midplane radius

0.87 m plasma end ellipticity radius

0.9 m first wall inner radius

2.00 m fission mantle outer radius

2.10 m (old and new) coil inner radius

2.89 m new coil system maximum coil outer radius

3.07 m old coil system maximum quadrupolar coil outer radius

4.35 m old coil system maximum axisymmetric coil outer radius

Fig. 8 A cross sectional comparison between the size of the old coil system and the new coil system, where the cross sectional area of the largest coil of the new coil system is about 27% of the combined cross sectional area (quadrupolar coil + circular coil) of the largest old coils. The size difference is to a large extent due to the lower magnetic field for the new coil system and the larger current density assumed in the coils, but the one-layer solution of the 3D coils also contributes to the compactness of the solution

is 4.35 m in the old design and in the new design it is reduced to 2.89 m. The new coil set is significantly smaller, and is in one layer only which means that there are fewer coils. This will reduce the cost of the coil system.

There is no need to round off sharp angles in the new coil set, as there were in the old coil set. It is not expected that the moderate curvature of these coils will cause problems for the superconductors. The 3D coils are standalone which makes them easier to handle and transport. The quadrupolar coils of the old coil system are coupled. Also, the maximum magnetic field is expected to be low for the coils, and most coils can be made of NbTi which is considerably cheaper than Nb_3Sn. Some coils at the mirror peak may need to be made of Nb_3Sn or Nb_3Al, which may increase their size somewhat. It is expected that they can be fitted in in that case. The strain in the coils has not been examined in detail yet.

The lower magnetic field will increase the required maximum β from about 20% to about 50% to achieve the

maximum fusion neutron production of $n_n = 7.1 \times 10^{18}$ neutrons/s for the 1.5 GWth option in Ref. [4]. The desired neutron production and thus the β would vary with the fission fuel burnup during a fuel cycle if the total output power should remain constant. Mirrors are known to be able to produce higher β values (GDT about 60% [23], and 2XIIB more than unity [24]), but the high β will deteriorate

the MHD stability of the plasma [25] and a more detailed examination is needed to fully address the finite β effects. There are also other stabilizing effects, such as finite Larmor radius effects [26] and the extra stability gained from the magnetic expanders [23]. Ballooning modes are not addressed in this work, partly since the authors of Ref. [26] do not believe that they will be β-limiting in (tandem) mirrors.

The design of the magnetic expander is not carried out in detail. There is a strong cancellation in the magnetic field at the magnetic expander, and it is probably necessary to have in situ adjusted correction coils at the expander to distribute the plasma load evenly on the plasma receiving "divertor plates".

In this design, neoclassical transport is partly addressed through the use of the omnigenious SFLM field in the central part of the confinement region. There will, however, be drifts in the other parts of the confinement region, and small drifts from the field inaccuracies caused by the coil system.

There is a possibility to optimize the coils with a numerical optimization method, for example similar to the one used in Ref. [1]. It is probably possible to find a coil set with that reproduces the ideal field with somewhat better accuracy. The current solution is, however, considered satisfactory, and the small deviances from the ideal field are not considered important. The 2% "ripple" seen in Fig. 6a is not a ripple in the ordinary sense since the magnetic field is increasing in this region and there are no regions where particles will be locally trapped. The "ripple" is merely a small modification of the magnetic field. If there should arise a need to reduce the deviations, they could also be considerably reduced by the use of ferromagnetic inserts [27].

Conclusions

A 3D single layer coil set for a low-field version of the SFLM Hybrid has been computed that reproduces the desired magnetic field with satisfying accuracy, and such a coil set can probably be realized with known technology. The set consists of 30 coils of a type which we have named "fish-bone coil" due to its resemblance of a fish skeleton when several coils are added. The coils are somewhat similar to a baseball coils with skewed sides. The coil set would be considerably cheaper than the earlier design described in Ref. [1]. The largest coil outer radius is reduced from 4.35 m in the old coil set to 2.89 m in the new design.

References

1. A. Hagnestål, O. Ågren, V.E. Moiseenko, J. Fusion Energ. **30**, 144 (2011)
2. O. Ågren, V.E. Moiseenko, K. Noack, A. Hagnestål, Fusion Sci. Technol. **57**, 326 (2010)
3. L. Wegener, J.-H. Feist, J. Sapper, F. Kerl, F. Werner, Fusion Eng. Des. **58–59**, 225 (2001)
4. K. Noack, V.E. Moiseenko, O. Ågren, A. Hagnestål, Ann. Nucl. Energ **38**, 578 (2011)
5. H. Bethe, Phys. Today **32**, 44 (1979)
6. S.L. Bogart, ERDsA-4, "DCTR Fusion-Fission Energy Systems Review Meeting", Germantown, Md. December 3–4, 1974, U.S. ERDA Report ERDA-4, U.S. Goverment Printing Office (1975)
7. See National Technical Information Service Document No. DE86010981 (R.W. Moir, J.D. Lee, D.H. Lee, D.H. Berwald, E.T. Cheng, J.G. Delene and D. L. Jassby, Fusion-Fission Hybrid Studies in the United States, 1986). Copies may be ordered from the National Technical Information Service, Springfield VA 22161 or via the web site http://www.osti.gov/bridge. Also available via the web site https://library-ext.llnl.gov (R.W. Moir, J.D. Lee, D.H. Lee, D.H. Berwald, E.T. Cheng, J.G. Delene and D. L. Jassby, LLNL UCRL-94306)
8. Ralph Moirs homepage, http://ralphmoir.com/aFusFisHyb.htm
9. S. Taczanowski, G. Domanska, J. Cetnar, Fusion Eng. Des. **41**, 455 (1998)
10. W. Manheimer, J. Fusion Energy **23**, 223 (2004)
11. W.M. Stacey, J. Mandrekas, E.A. Hoffman, G.P. Kessler, C.M. Kirby, A.N. Mauer, J.J. Noble, D.M. Stopp, D.S. Ulevich, Fusion Eng. Des. **63–64**, 81 (2006)
12. Y. Wu, S. Zheng, X. Zhu, W. Wang, H. Wang, S. Liu, Y. Bai, H. Chen, L. Hu, M. Chen, Q. Huang, D. Huang, S. Zhang, J. Li, D. Chu, J. Jiang, Y. Song, Fusion Eng. Des. **81**, 1305 (2006)
13. M. Kotschenreuther, P.M. Valanju, S.M. Mahajan, E.A. Schneider, Fus. Eng. Des. **84**, 83 (2009)
14. K. Noack, A. Rogov, A.A. Ivanov, E.P. Kruglyakov, Y.A. Tsidulko, Ann. Nucl. Energ. **35**, 1216 (2008)
15. V.G. Kotenko, V.E. Moiseenko, *Problems of Atomic Science and Engineering, series Thermonuclear Fusion* (*Voprosy Atomnoi Nauki i Tekhniki, Ser. Termoiadernyi Sintez*), vol. 3 (2011), pp. 74–80. (in Russian).
16. R.W. Moir, N.N. Martovetsky, A.W. Molvik, D.D. Ryutov, T.C. Simonen, LLNL-report LLNL-TR-484071, available at http://ralphmoir.com/aFusFisHyb.htm
17. H. Yapici, N. Demir, G. Genç, J. Fusion Energ. **27**, 206 (2008)
18. K. Noack, O. Ågren, J. Källne, A. Hagnestål, V.E. Moiseenko, submitted to the Varenna conference FUNFI (2011)
19. K. Yoshida, K. Kizu, K. Tsuchiya, H. Tamai, M. Matsukawa, M. Kikuchi, A. della Corte, L. Muzzi, S. Turtù, A. Di Zenobio, A. Pizzuto, A. Portafaix, S. Nicollet, B. Lacroix, P. Decool, J.-L. Duchateau, L. Zani, IEEE Trans. Appl. Superconduct. **18**, 441 (2008)
20. T.B. Kaiser, L.D. Pearlstein, Phys. Fluids **26**, 3053 (1983)
21. J. A. Bradshaw, IEEE Trans. Plasma Sci. PS-6, 166 (1978)
22. R.W. Moir, R.F. Post, Nucl. Fusion **9**, 253 (1969)
23. T.C. Simonen, A. Anikeev, P. Bagryansky, A. Beklemishev, A. Ivanov, A. Lizunov, V. Maximov, V. Prikhodko, Yu. Tsialko, J. Fusion Energ. **29**, 558–560 (2010)

24. See National Technical Information Service Document No. UCRL81555 (T.K. Fowler, The US Mirror Program, 1978). Copies may be ordered from the National Technical Information Service, Springfield VA 22161 or via the web site www.ntis.gov. Also available via the web site https://library-ext.llnl.gov (T.K. Fowler, LLNL UCRL-81555)

25. D.A. D'ippolito, G.L. Francis, J.R. Myra, Plasma Phys. Control. Fusion **27**, 517–522 (1985)

26. W.M. Newins, L.D. Pearlstein, Phys. Fluids **31**, 1988 (1988)

27. See National Technical Information Service Document No. DE85010042 (G.W. Hamilton, Magnetic Ripple Correction in Tandem Mirrors by Ferromagnetic Inserts, 1985). Copies may be ordered from the National Technical Information Service, Springfield VA 22161 or via the web site www.ntis.gov. Also available via the web site https://library-ext.llnl.gov (G.W. Hamilton, LLNL UCRL-90617)